# Drying-induced bending deformation of cellulose nanocrystals studied by molecular dynamics simulations

Yu Ogawa, Yoshiharu Nishiyama, Karim Mazeau

# Drying-induced bending deformation of cellulose nanocrystals studied by molecular dynamics simulations

Yu Ogawa,* Yoshiharu Nishiyama,* Karim Mazeau

Univ. Grenoble Alpes, CNRS, CERMAV, 38000, Grenoble, France

*Corresponding authors: (Y.O.) yu.ogawa@cermav.cnrs.fr

(Y.N.) yoshiharu.nishiyama@cermav.cnrs.fr

ORCID: (Y.O.) 0000-0003-0677-7913 (Y.N.) 0000-0003-4069-2307

**ABSTRACT**

Drying cellulosic materials from their water-swollen state can collapse their ultrastructure and alter their macroscopic material properties such as mechanical strength and water-retention ability. However, at the single-crystal or molecular level, little is known about the deformation of cellulose upon drying. We thus investigate herein the drying-induced deformation of a cellulose crystal by using an atomistic molecular dynamics simulation that considers a hydrated system composed of two short cellulose crystals, a lower one fixed to a flat substrate and an upper one free to deform. To mimic vacuum drying, the water is gradually removed from the system. As the drying proceeds, the upper cellulose crystal bends and forms a tight contact with the lower cellulose crystal. This result underlines the importance of lateral deformation of cellulose crystals in the collapse of the cellulose ultrastructure and provides insights into the molecular mechanisms responsible for modifying the properties of cellulose materials.

**Keywords**: cellulose; drying; lateral deformation; molecular dynamics

## INTRODUCTION

Cellulose is extracted and processed in the aqueous condition in many industrial processes, from chemical pulping to fiber and textile production to nanocellulose production. As a result, producing cellulosic materials often requires drying or water removal. Drying cellulosic materials modifies its physical properties; for instance, in the process of paper manufacturing, pulp fibers stiffen and shrink laterally upon drying (Minor, 1994; Giacomozzi and Joutsimo, 2017). In addition, once dried, the pulp does not fully recover to the original state upon rewetting, and repeated drying and wetting produces a more rigid and brittle material. This phenomenon, called “hornification,” poses a challenge to paper recycling because hornified fibers do not reswell to their initial hydrated state when resuspended in water, which weakens recycled paper. Such degradation of the material properties upon conventional drying (air, oven, contact, etc.) occurs not only with pulp fibers but also with different cellulosic materials such as hydrogels and nanocellulose materials (Peng et al., 2012; Rämänen et al., 2012). Retaining the fine structure of cellulosic materials and minimizing the impact of drying often requires more gentle and costly drying methods such as freeze-drying or critical-point drying (Jin et al., 2004; Heath and Thielemans, 2010; Hoepfner et al., 2008; Beaumont et al., 2017). Conversely, simple air drying also produces some exceptional material properties in cellulosic materials. For example, a cast film of cellulose nanofiber dried from an aqueous suspension forms an exceptionally high barrier against oxygen gas (Fukuzumi et al., 2009), which means that this simple drying method packs the cellulose nanofibers tightly enough to prevent gas molecules from permeating through the film.

These drying-induced modifications in the mechanical properties are due to microscopic, irreversible structural changes within cellulosic materials and at various length

scales (Hult et al., 2003; Newman, 2004; Oksanen et al., 1997). Given that, compared with the rigidity of cellulose the surface tension of water is very significant at the nanometric scale, the capillary force can collapse the ultrastructures such as micropores and nanofiber networks, as has been observed by using various analytical techniques (e.g., microscopy, nitrogen adsorption, solid-state NMR spectroscopy, differential scanning calorimetry) (Häggkvist et al., 1998; Lovikka et al., 2016; Park et al., 2006). Although this interpretation of the drying effect is well accepted, what remains unclear is how cellulose deforms at the single-crystal and molecular levels in these collapsed structures. Recent reports based on transmission electron microscopy and scanning probe microscopy testify to the increasing interest in the nanoscale deformation of cellulose crystals (Mattos et al., 2019; Ogawa, 2019; Smith et al., 2019). Unfortunately, limitations in characterization methods (e.g., spatial resolution) and the intrinsic heterogeneity of cellulose morphology hinder the understanding of such deformations on a molecular level. More detailed molecular-level descriptions are thus needed to fully understand the deformation mechanism of cellulose crystals and how it affects material properties.

We recently demonstrated that, for cellulose crystals, force-field-based atomistic simulations provide structural insights into various deformation modes such as shear and bending deformations (Chen et al., 2016; 2018; Molnár et al., 2018). These computational studies indicate that crystalline cellulose is highly pliant in its lateral plane, contrary to the general assumption that crystalline cellulose forms rigid rods. In the present study, we use atomistic molecular dynamics (MD) to simulate a simplified system to determine the deformation of cellulose crystals upon drying. The results indicate that crystalline cellulose undergoes a bending deformation upon gradual removal of water from a hydrated system composed of two short cellulose crystals.

## COMPUTATIONAL METHODS

### Simulation setup

All simulations were done with GROMACS (Abraham et al., 2015) using the GROMOS 56Acarbo force field (Hansen and Huenenberger, 2011), including the optimized Lennard-Jones repulsive parameter for the united CH1 atom type (Chen et al., 2014). This optimized GROMOS force field has already been used to investigate the lateral deformation of cellulose crystals in vacuum, which is similar to the simulation presented herein (Chen et al., 2016; Molnár et al., 2018). Although not designed specifically to model such a solid-vacuum interface, the deformation of cellulose crystals given by the force field is quantitatively consistent with the results of finite-element analysis and qualitatively consistent with transmission electron microscopy observations of kinked cellulose crystals (Chen et al., 2016). Thus, we believe that it can reproduce the deformation of cellulose crystals induced by dehydration.

MD simulations were done in the *NVT* ensemble with a 2 fs integration time step. The stochastic velocity-scaling algorithm of Bussi et al. (2007) was used to maintain the temperature at 300 K, and O-H bonds were constrained by using the LINCS algorithm (Hess et al., 1997). The long-range electrostatic interactions and Lennard-Jones interactions were both calculated by using the cutoff method with a cutoff distance of 0.9 nm. The analyses were done by using GROMACS and in-house scripts. The MD structures were visualized by using PyMOL (PyMOL ver. 2.1.0).

### Model construction

95 The cellulose microfibril model of the major native allomorph Iβ was built from crystal
96 structures (Nishiyama et al., 2002) by considering the dominant hydrogen-bond network,
97 pattern A. The crystal had dimensions of approximately 3.5 nm × 3.5 nm × 20 nm and
98 consisted of 36 chains (6 x 6), each 40 residues long, exposing the (1 1 0) and (1 −1 0)
99 surfaces. Note that the crystal width is similar to that of higher plant cellulose microfibrils
100 (≈3 nm), whereas the crystals are much shorter than natural cellulose microfibrils.
101 This crystal model was duplicated and two crystals were positioned parallel to each
102 other, separated by 1.8 nm, in a small simulation box (4.5 × 9.5 × 22 $nm^3$), as shown in Fig.
103 1a. The system was then solvated with simple-point-charge water (Berendsen et al., 1981),
104 and the energy was minimized by using the steepest descent method followed by the
105 conjugate gradient method, with the convergence criterion being a maximum force of
106 10 kJ $mol^{-1}$ $nm^{-1}$. The positions of the selected atoms were then constrained as shown in Fig.
107 1b to maintain the separation between the central sections of the crystals, and this position
108 constraint was retained in the following MD simulations. The system was then stepwise
109 heated in the *NPT* ensemble from 0 to 300 K in 20 ns. The pressure was regulated by using a
110 Berendsen barostat with a relaxation time of 2.0 ps (Berendsen et al., 1984).
111
112 **General strategy for modeling the drying process**
113 To demonstrate the drying-induced deformation of cellulose, we studied the simple
114 model shown in Figure 1. As illustrated in Fig. 1a, we considered a geometry where an upper
115 cellulose crystal is positioned parallel to and above another crystal laid on a flat substrate,
116 and a crystal is sandwiched crossways between the two parallel crystals to maintain a
117 constant separation between them. We used this crossed-fibril geometry to mimic the
118 random orientation of cellulose crystals in a film drop-casted from aqueous suspensions

(Fukuzumi et al., 2009). In the model studied, all atomic positions in the bottom crystal were constrained except those at the upper surface that faced the upper crystal. The third crystal was treated implicitly to reduce the system size. The inter-crystal spacing was maintained by constraining the atomic positions of four residues at the center of each molecular chain on the bottom layer of the upper crystal. The side surfaces of the cellulose crystals were hydrophilic (1 −1 0) and (1 1 0), and the surfaces facing the opposing crystal were both (1 1 0) surfaces.

Water evaporation was modeled by stepwise removal of water molecules in the gas phase. First, the hydrated system was heated to 300 K, and then the volume of the simulation box was expanded fourfold (10 × 15 × 25 nm) to generate vacuum space. The MD simulation was then executed at a constant volume at 300 K but was stopped every 100 ps to remove isolated water molecules ("isolated" water molecules were defined as those with no neighbor molecule within 1 nm). Upon restarting the simulation, the atomic velocities from the previous MD trajectory were retained, so the system temperature remained essentially constant at 300 K.

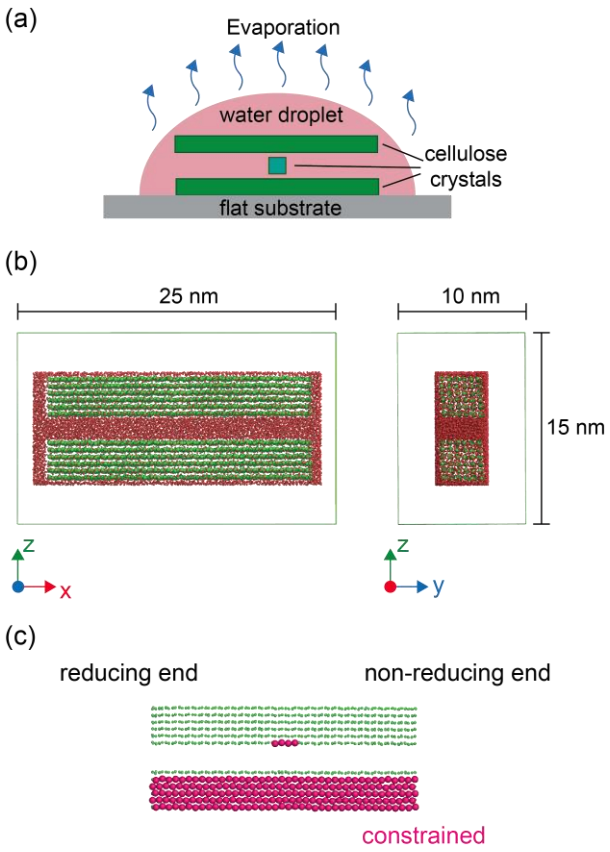


**Figure 1.** Model used to simulate drying of cellulose crystals: (a) Schematic drawing showing geometry of simulation. (b) Initial dimensions of simulation box containing two crystals and water molecules. For clarity, only the C1 atoms of cellulose (green) and the oxygen atoms of water (red) appear in these snapshots. (c) Constraints on atomic positions within cellulose crystals. The positions of the magenta glucose residues were constrained in the x, y, and z directions. For simplicity, only C1 atoms (green) are shown for each residue, but the constraints were applied to all atoms in the residues. The left and right extremities of the upper (lower) surface of the lower (upper) cellulose crystal are called the reducing and non-reducing ends, respectively. The cellulose crystals are maintained in this orientation in all figures presented herein.

## RESULTS AND DISCUSSION

Figure 2 summarizes the general features of the drying process. As shown in Fig. 2a, the number of water molecules decreases monotonically in time, indicating that the strategy adopted is suitable for simulating the gradual removal of water on the nanometer scale. Almost all water molecules are removed after 340 ns (32 and 8 water molecules remain at 340 and 350 ns, respectively). Figure 2b shows snapshots of the simulated system during the drying process and reveals a bending deformation of the upper cellulose crystal and the heterogeneous removal of water.

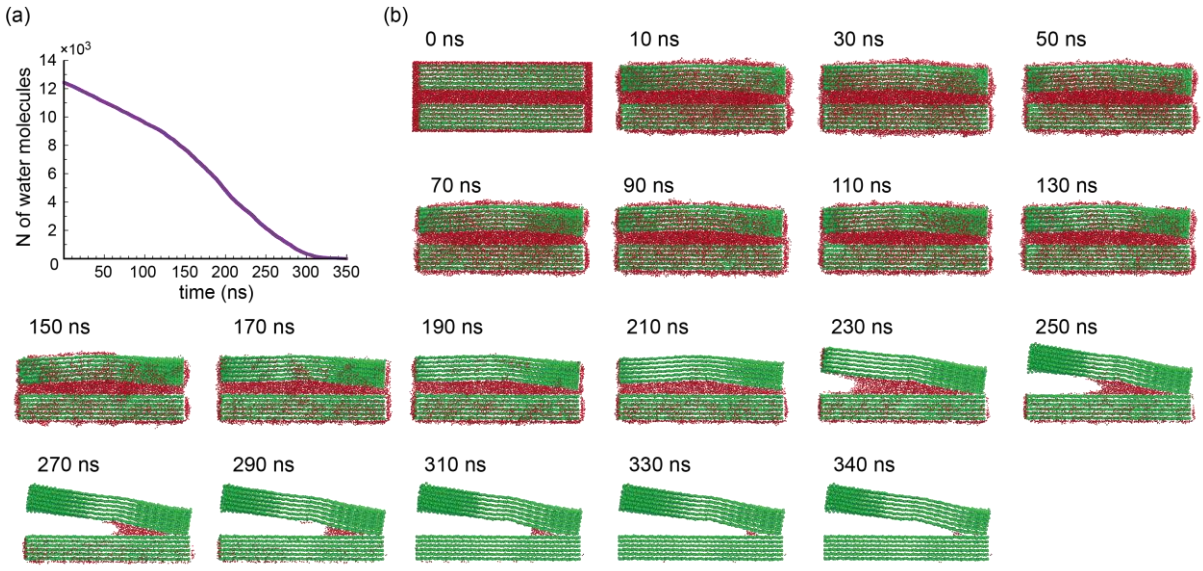


**Figure 2.** Result of drying simulation: (a) Number of water molecules as a function of time. (b) Snapshots of simulated cellulose-crystal system during drying.

**Deformation of cellulose crystal**

At 10 ns, the upper cellulose crystal deforms from its initial linear form into a continuous curve (Fig. 3a). This deformation occurs immediately upon starting the simulation as can be seen in the bending angle evolution in Fig. 3b. The curved morphology is imposed by the water droplet to minimize the area of the liquid surface. This result

164 indicates that the surface tension of water suffices to cause a lateral deformation of very
165 short cellulose crystals. At this point, the upper cellulose crystal becomes convex with
166 respect to the lower cellulose crystal and roughly symmetric with respect to the center of
167 the crystal (Fig. 3b).

168 The curved morphology persists until about 150 ns, at which point most water
169 molecules have been removed from the upper and side faces of the upper crystal. After
170 170 ns the crystal becomes asymmetrically bent about its center. The lower crystal surface
171 at the non-reducing end (right-hand end) approaches to within significantly less than 0.9 nm
172 of the upper surface of the bottom crystal, which is the cutoff distance for non-bonding
173 interactions in this simulation. At 220 ns (Fig. 3), the edge of the non-reducing end of the
174 upper crystal makes contact with the bottom crystal. The bending angle of the upper crystal
175 increases from 4° in the initial curved state (i.e., at 10 ns) to 10°. The reducing end of the
176 upper crystal has moved upward, away from the bottom crystal. This displacement of the
177 reducing end is initiated by the rupture of the continuous water layer that previously forced
178 the curved morphology of the upper crystal. As the drying proceeds further, the crystal-
179 contact area expands and produces surface-to-surface contact (Figs. 3a and 4b). After 240
180 ns, this contact area remains constant because the bending angle for the non-reducing end
181 remains constant once the contact area is well established. In contrast, the bending angle of
182 the free reducing end fluctuates (Fig. 3b). The non-reducing end of the upper crystal forms a
183 concave curvature. As detailed below, the water molecules between the two crystals are
184 expelled from the contact area.
185

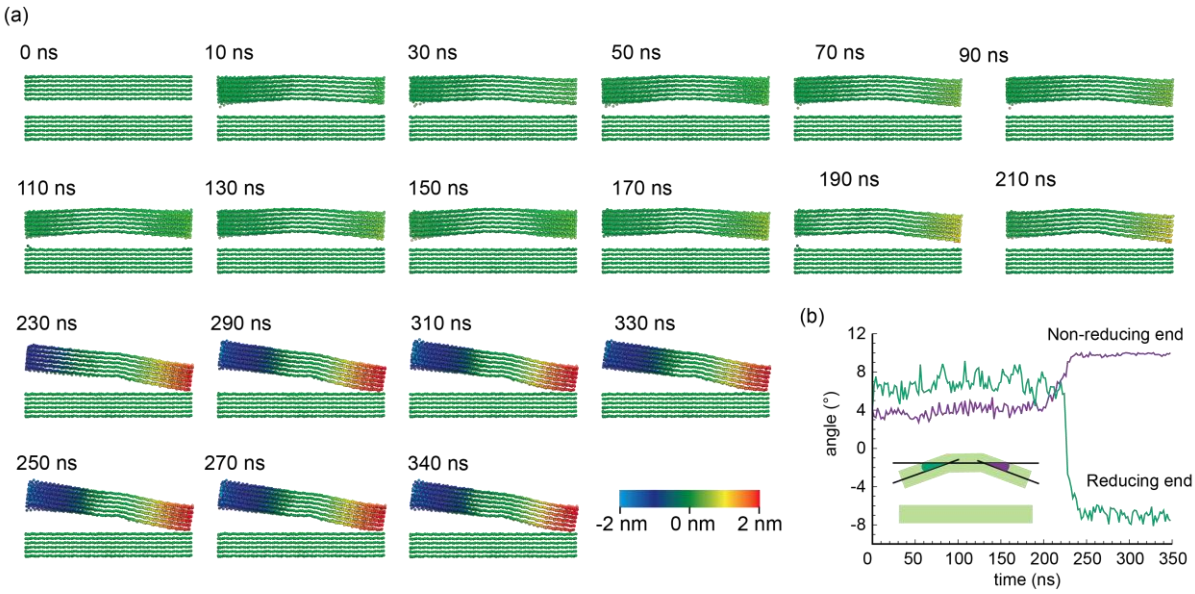


**Figure 3.** (a) Deformation of upper cellulose crystal in drying simulation. The color code indicates the atomic displacement in the *z* direction (vertical direction in the figure). (b) Bending angle plotted as a function of time during drying for upper cellulose crystal at reducing end (green) and non-reducing end (purple). The bending angles are the angles between the tangent to the central section and the tangents to the ends of the crystal, as schematized in the inset.

**Water removal**

Immediately after the simulation box expands fourfold in volume, the surface tension of water causes the water molecules to form an elongated droplet surrounding the two cellulose crystals (Fig. 2). The water molecules gradually evaporate from the outer side of the droplet, whereas the number of water molecules trapped between the cellulose crystals remains roughly constant. As mentioned above, most of the water molecules around the crystals have evaporated after 170 ns, leaving only a monolayer of water molecules directly adsorbed on the cellulose-crystal surfaces. As seen in Fig. 2a, the evaporation rate increases at this stage. Such evaporative behavior is evocative of a type-II isotherm, implying that a

strong interaction exists between the cellulose-crystal surface and the water. The position constraints that lead to a temperature of 0 K for the constrained part of the crystal means that water adsorbed on the bottom crystal evaporates much more slowly than water adsorbed on the upper crystal.

Once the contact between the cellulose crystals occurs at 220 ns, a water meniscus forms on the reducing end where the two crystals are widely separated (Fig. 4a). The meniscus is concave, which is indicative of strong adhesion between water and the cellulose-crystal surfaces. As the drying proceeds further, the water molecules evaporated from the reducing end (i.e., the left side where the crystals are separated), and the meniscus surface gradually moves toward the non-reducing end where the cellulose crystals are in contact. The water molecules are retained in this opening until the end of the drying process, as indicated by the few molecules still apparent at 340 ns in Fig. 3.

Conversely, the water molecules near the contact area between the two crystals are expelled independently of the drying within the open space between the reducing ends of the cellulose crystals. Figure 4b shows a series of close-up snapshots of the contact area. As mentioned above, the crystals make contact after about 210 ns, at which point only the edge of the upper crystal touches the upper surface of the bottom crystal. In the following 20 ns, the water molecules move away from this contact line, inducing direct contact between the two cellulose-crystal surfaces. This direct contact leads to the formation of hydrogen bonds between the two cellulose-crystal surfaces, as shown in Fig. 4c. From 210 to 240 ns, the number of hydrogen bonds rapidly increases as water is removed from the contact area; beyond 240 ns, this number increases slowly, indicating a further extension of the contact area. These hydrogen bonds likely contribute to further stabilizing the contact between the two cellulose crystals.

Water is removed from the contact area much faster than in the adjacent open space between the two cellulose crystals, despite the two surfaces in the contact being hydrophilic. Previous atomistic MD simulations of similar duration indicate that water molecules are often incorporated into aggregates of cellulose crystals in the aqueous condition (Chen et al., 2019; Paajanen et al., 2019). The asymmetric geometry at the drying front induces compressive stress at the extremity where the crystals touch each other, which would also contribute to squeezing out water rather than evaporative drying. This removal of water molecules from between the cellulose crystals and the subsequent tight adhesion of the cellulose surfaces is presumably the main factor on the nanometric scale that causes the collapse of the cellulose structure upon drying.

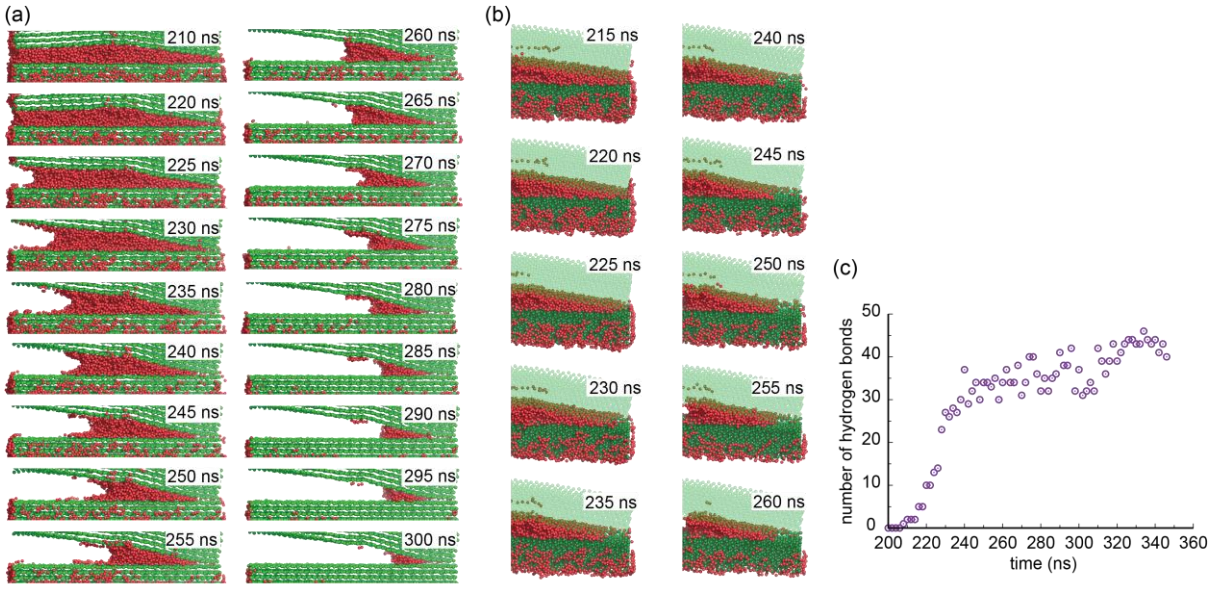


**Figure 4.** (a) Formation of water meniscus between two cellulose crystals. (b) Removal of water from the contact area between the two crystals. The upper crystal is translucent to reveal the water molecules between the crystals. (c) Number of hydrogen bonds between the two cellulose-crystal surfaces as a function of time.

## CONCLUSIONS

By using atomistic MD simulations of a simplified cellulose-crystal system in water, we show that drying may cause a significant bending deformation of a cellulose crystal and a tight adhesion between cellulose-crystal surfaces, even without external forces. The simulation shows that the crystal bending occurs not only because of the adhesion between cellulose crystals but also because of the surface tension of the surrounding water. The formation of a concave water meniscus in the opening between the two crystals is indicative of strong interactions between cellulose and water, and the water molecules are quickly excluded from the contact area between the two crystals. Such preferential drying between two crystals leads to adhesion between the cellulose surfaces.

The deformation of the upper cellulose crystal constitutes a complex phenomenon induced by the interplay between the cellulose crystals and water molecules, and the details of the simulated deformation may depend not only on the force-field parameters but also on the simulation conditions. Thus, the evolution of the deformation should be compared and verified with experimental observations such as atomic force microscopy images of deformed cellulose crystals. Such a comparison should allow a more complete understanding of the nanoscale structural modifications that are at the origin of the property changes of cellulosic materials.

**Acknowledgment**

We acknowledge the computational resources of the Centre d'Expérimentaion et de Calcul Intensif (CECIC) at the Institut de Chimie Moléculaire de Grenoble (ICMG) of the University Grenoble Alpes.

**References**

268 Abraham MJ, Murtola T, Shulz R, Páll S, Smith JC, Hess B, Lindahl E (2015) GROMACS: high
269 performance molecular simulations through multi-level parallelism from laptops to
270 supercomputers. SoftwareX 1-2:19-25
271 Beaumont M, König J, Opietnik M, Potthast A, Rosenau T (2017) Drying of a cellulose II gel:
272 effect of physical modification and redispersibility in water. Cellulose 24:1199-1209
273 Berendsen HJC, Postma JPM, van Gunsteren WF, Hermans J (1981) Interaction models for
274 water in relation to protein hydration. In Intermolecular Forces; Pullman, B., Ed.;
275 Springer: Dordrecht, pp 331-342.
276 Berendsen HJC, Postma JPM, van Gunsteren WF, DiNola A, Haak JR (1984) Molecular
277 dynamics with coupling to an external bath. J Chem Phys 81:3684-3690.
278 Bussi G, Donadio D, Parrinello M (2007) Canonical sampling through velocity rescaling. J
279 Chem Phys 126:014101/1-014101/7
280 Chen P, Nishiyama Y, Mazeau K (2014) Atomic partial charges and one Lennard-Jones
281 parameter crucial to model cellulose allomorphs. Cellulose 21:2207-2217
282 Chen P, Ogawa Y, Nishiyama Y, Ismail AE, Mazeau K (2016) Linear, non-linear and plastic
283 bending deformation of cellulose nanocrystals. Phys Chem Chem Phys 18: 19880-
284 19887
285 Chen P, Ogawa Y, Nishiyama Y, Ismail AE, Mazeau K (2018) Iα to Iβ mechano-conversion and
286 amorphization in native cellulose simulated by crystal bending. Cellulose 25:4345-
287 4355
288 Chen P, Terrenzi C, Furó I, Berglund LA, Wohlert J (2019) Quantifying localized
289 macromolecular dynamics within hydrated cellulose fibril aggregates. Macromolecules
290 52: 7278-7288

291 Fukuzumi H, Saito T, Iwata T, Kumamoto Y, Isogai A (2009) Transparent and high gas barrier
292 films of cellulose nanofibers prepared by TEMPO mediated oxidation.
293 Biomacromolecules 10:162-165
294 Giacomozzi DE, Joutsimo O (2017) Drying temperature and hornification of industrial never-
295 dried *Pinus radiata* Pulps. 2. Voith Sulzer Refining. BioResources 12:1532-1547
296 Häggkvist M, Li TQ, Ödberg, L (1998) Effects of drying and pressing on the pore structure in
297 the cellulose fibre wall studied by $^{1}H$ and $^{2}H$ NMR relaxation. Cellulose 5:33-49
298 Hansen HS, Huenenberger PH (2011) A re-optimized GROMOS force field for hexopyranose-
299 based carbohydrates accounting for the relative free energies of ring conformers,
300 anomers, epimers, hydroxymethyl rotamers, and glycosidic linkage conformers. J
301 Comput Chem 32:998-1032
302 Heath L, Thielemans W (2010) Cellulose nanowhisker aerogels. Green Chem 12:1448-1453
303 Hess B, Bekker H, Berendsen HJC, Fraaije JGEM (1997) LINCS: a linear constraint solver for
304 molecular simulations. J Comput Chem 18:1463-1472
305 Hoepfner S, Ratka L, Milow B (2008) Synthesis and characterization of nanofibrillar cellulose
306 aerogels. Cellulose 15:121-129
307 Hult EL, Larsson PT, Iversen T (2001) Cellulose fibril aggregation - an inherent property of
308 kraft pulps. Polymer 42: 3309-3314
309 Jin H, Nishiyama Y, Wada M, Kuga S (2004) Nanofibrillar cellulose aerogels. Colloids Surf A
310 240:63-67
311 Lovikka VA, Khanjani P, Väisänen S, Vuorinen T, Maloney TC (2016). Porosity of wood pulp
312 fibers in the wet and highly open dry state. Microporous Mesoporous Mater 234:326-
313 335.

314 Mattos BD, Tardy BL, Rojas OJ (2019) Accounting for substrate interactions in the
315 measurement of the dimensions of cellulose nanofibrils. Biomacromolecules 20:2657-
316 2665
317 Minor JL (1994) Hornification – Its origin and meaning. Progress in paper recycling 3:93-95
318 Molnár G, Rodney D, Martoïa F, Dumont PJJ, Nishiyama Y, Mazeau K, Orgéas L (2018)
319 Cellulose crystals plastify by localized shear. Proc Natl Acad Sci U.S.A. 115:7260-7265
320 Newman RH (2004) Carbon-13 NMR evidence for cocrystallization of cellulose as a
321 mechanism for hornification of bleached kraft pulp. Cellulose 11: 45-52
322 Nishiyama Y, Langan P, Chanzy H (2002) Crystal structure and hydrogen-bonding system in
323 cellulose Iβ from synchrotron X-ray and neutron fiber diffraction. J Am Chem Soc
324 124:9074-9082
325 Ogawa, Y (2019) Electron microdiffraction reveals the nanoscale twist geometry of cellulose
326 nanocrystals. Nanoscale 11:21767-21774
327 Oksanen T, Buchert J, Viikari L (1997) The role of hemicelluloses in the hornification of
328 bleached kraft pulps. Holzforschung 51:355-360
329 Paajanen A, Ceccherini S, Maloney T, Ketoja JA (2019) Chirality and bound water in the
330 hierarchical cellulose structure. Cellulose 26:5877-5892
331 Park S, Venditti RA, Jameel H, Pawlak JJ (2006) Changes in pore size distribution during the
332 drying of cellulose fibers as measured by differential scanning calorimetry. Carbohydr
333 Polym 66:97-103.
334 Peng Y, Gardner DJ, Han Y (2012) Dryomg cellulose nanofibrils: in search of a suitable
335 method. Cellulose 19:91-102
336 PyMOL, The PyMOL Molecular Graphics System, Version 2.1.0 Schrödinger, LCC.

337 Rämänen P, Penttilä P, Svedström K, Maunu SL, Serimaa R (2012) The effect of drying
338 method on the properties and nanoscale structure of cellulose whiskers. Cellulose
339 19:901-912
340 Smitåh KB, Tisserant J-N, Assenza S, Arcari M, Nyström G, Mezzenga R (2019) Confinement-
341 induced ordering and self-folding of cellulose nanofibrils. Adv Sci 6:1801540.
342 DOI:10.1002/advs.201801540